Supplementary Information

A quantum dot intercalated robust covalent organic framework membrane for ultrafast proton conduction

Chunyang Fan[a,b]†, Quan Peng[a,b]†, Hong Wu[a,b,c*], Benbing Shi[a,b], Xiaoyao Wang[a,b], Chumei Ye[a,b], Yan Kong[a,b], Zhuoyu Yin[a,b], Yiqin Liu[a,b], Zhongyi Jiang[a,b,d*]

[a] Key Laboratory for Green Chemical Technology of Ministry of Education, School of Chemical Engineering and Technology, Tianjin University, Tianjin 300072, China

[b] Collaborative Innovation Center of Chemical Science and Engineering (Tianjin), Tianjin, 300072, China

[c] Tianjin Key Laboratory of Membrane Science and Desalination Technology, Tianjin University, Tianjin 300072, China

[d] Joint School of National University of Singapore and Tianjin University, International Campus of Tianjin University, Binhai New City, Fuzhou, 350207, China

† These authors contributed equally.

Experimental

Materials.

1,3,5-Triformylphloroglucinol was bought from Jilin Chinese Academy of Sciences - Yanshen Technology Co., Ltd. and 2,5-diaminobenzenesulfonic acid was bought from TCI (Shanghai) Development Co., Ltd. Citric acid and octanoic acid were bought from Shanghai Aladdin Technology Co., Ltd. Alendronate sodium was bought from Xiya Chemical Technology (Shandong) Co., Ltd. All regents and solvents were used as received without any further purification.

Synthesis of graphene quantum dot and phosphorylated graphene quantum dot

Graphene quantum dot (GQD) was prepared by thermal polymerization of citric acid according to the reported literature. Typically, 2 g citric acid was reacted in the oven at 200 °C for 15 min and then cooled to room temperature in the air. The obtained yellow solid was dissolved in deionized water for purification. Specifically, the solution of GQD was undergone dialysis process for 1 day (molecular weight cut off: 3500 Da) and then treated by a dialysis process for another day (100 Da). The GQD powder was obtained by freeze-drying the purified GQD solution. Phosphorylated GQD (PGQD) was prepared by chemical modification of GQD with alendronate sodium. Typically, GQD (2 g) and excess alendronate sodium were dissolved in 30 mL of deionized water, and the resulting solution was poured into a Teflonlined stainless-steel autoclave. Then, the autoclave was heated in the oven at 200 °C for 24 h and then cooled to room temperature in the air. Finally, the PGQD was purified following the same procedure of GQD.

Preparation of sulfonated covalent organic framework nanosheets

The sulfonated covalent organic framework (SCOF) nanosheets were synthesized according to the reported literature. Typically, 1,3,5-Triformylphloroglucinol (21.0 mg, 0.1 mmol) was dispersed into octanoic acid (20 ml) and sonicated until completely dissolved. 2,5-diaminobenzenesulfonic acid (28.2 mg, 0.15 mmol) was dissolved in deionized water (30 ml) and sonicated until complete dissolution. Then, the solution of

2,5-diaminobenzenesulfonic acid was poured into a 100 ml beaker and the 1,3,5-Triformylphloroglucinol solution was slowly dropped above the amine solution. The beaker was sealed and placed in a constant temperature humidity chamber at 16 °C for 3 days without any disturbance. Finally, the as-prepared SCOF nanosheets solution was dialyzed in deionized water for 3 days.

Preparation of SCOF and SCOF/PGQD membranes

The SCOF/PGQD membranes were prepared by a vacuum-assisted self-assembly method on polyacrylonitrile (PAN) membrane. Typically, the SCOF nanosheets solution (1 ml) and sodium hydroxide solution (1 ml, 0.01 mmol/ml) were mixed together to obtain a uniform and clear solution. Then, the excess sodium hydroxide solution (0.01 mmol/ml) was dropped into a certain amount of PGQD solution (50, 100, 150, 200 μl) until the mixture became alkaline. The pretreated PGQD solution was added into the obtained alkaline SCOF solution and stirred for 0.5 h. Then, the SCOF/PGQD membranes were fabricated by filtrating the mixture solution on a PAN substrate. Notably, the resultant SCOF/PGQD membranes with PAN should be immersed in H_2SO_4 (1 M) for 5 minutes before transferring into the N, N-dimethylformamide (DMF) solution for the dissolution of PAN substrate. The free-standing SCOF/PGQD membranes were then soaked into deionized water to exchange the DMF. Finally, the SCOF/PGQD membranes were acidified by H_2SO_4 solution (1 M) for 24 h and then washed with lots of deionized water until the pH of the solution reached 7.0. The resultant membranes were named as SCOF/PGQD-X, where X denotes the mass percentage of PGQD to SCOF nanosheets of 12.5, 25, 37.5, and 50, corresponding to the volume of PGQD solution of 50, 100, 150, 200 μl respectively. For comparison, pure SCOF membrane was prepared following the same procedure of SCOF/PGQD-X membranes without the addition of PGQD.

Characterization and measurements.

Characterization

The Powder X-ray diffraction (PXRD) data were acquired by a Rigaku D/max 2500v/pc diffractometer. The Fourier transform infrared (FT-IR) spectra were measured with a BRUKER Vertex 70 spectrometer. UV absorbance curves were recorded on Thermo Scientific Evolution 220 UV-Visible Spectrophotometer. Surface zeta potentials were tested by Zetasizer nano ZS90. Solid-state ^{13}C NMR spectra were collected on Bruker 600 MHz NMR spectrometer (JEOL JNM ECZ600R). Scanning Electron Microscopy (SEM) images and Transmission Electron Microscopy (TEM) images were collected by field emission scanning electron microscope (Nanosem 430) and HRTEM (Tecnai G2 F20), respectively. Atomic force microscopy (AFM) image was obtained by BRUKER Dimension Icon. The thermal property of the membrane samples was measured through thermogravimetric analysis (TGA, NETZSCH-TG 209 F3) with ramp rate of 10 °C min^{-1} (N_2 atmosphere, 40-800 °C). The mechanical property of membrane samples was evaluated by the electronic universal testing equipment (Yangzhou Zhongke WDW-02, 5 mm min^{-1}).

Proton conductivity of the membranes Measurement

The proton conductivities (σ, S cm^{-1}) of membrane samples were measured using a two-probe conductivity cell equipped with an impedance analyzer (PARSTAT4000). A signal amplitude of 15 mV operating over the frequency range from 1 MHz to 0.1 Hz was utilized in the experiment. The temperature and relative humidity (RH) were controlled by a temperature and humidity-controlled chamber. The proton conductivity can be calculated by formula given below:

$$\sigma = \frac{l}{AR} \qquad (1)$$

where l (cm) refers to the distance between the two platinum electrodes; R is the impedance at given temperature and RH (Ω). And A is the cross-sectional area of the samples (cm^{-2}).

Water uptake and swelling ratio experiments

The water uptake and swelling ratio of membranes were measured at 30 °C and 60 °C and calculated as follows,

$$\text{Water uptake (\%)} = \frac{W_1 - W_0}{W_0} \times 100 \quad (2)$$

$$\text{In - plane swelling ratio (\%)} = \frac{A_1 - A_0}{A_0} \times 100 \quad (3)$$

$$\text{Through - plane swelling ratio (\%)} = \frac{T_1 - T_0}{T_0} \times 100 \quad (4)$$

where the W_1, W_0 and A_1, A_0 represent the weight and area (length × width) of the wet (hydrated) and dry membranes, respectively. T_1 and T_0 are the thickness of wet and dry membranes. Each measurement was repeated three times and the standard deviation was within ± 5.0%.

Ion exchange capacity (IEC) measurements

IEC values refer to the molar quantities of exchangeable H^+ contained in a dried membrane sample per unit mass, which was determined by traditional titration method. A certain mass of the dried membrane (W_0, g) was immersed in NaCl solution (2.0 M) for 24 h until the H^+ was sufficiently replaced by Na^+. The solution was subjected to acid-base titration by standard NaOH solution (c mol L^{-1}), and the consumption (V_{OH}, mL) of the NaOH solution was recorded. Repeat the measurements three times for each sample. The IEC of the membranes could be obtained through formula given below.

$$\text{IEC} = \frac{1000 \times c \times V_{OH}}{W_0} \quad (5)$$

Oxidative stability tests

The oxidative stability of PGQD@TpPa-SO3H series membranes was assessed via immersion of a membrane in Fenton's reagent (aqueous solution containing 3% H_2O_2 and 2 ppm Fe^{2+}) at 80 °C for 1h. According to the residual weight, oxidative stability of COF membranes was conducted using the following equations:

$$\text{Oxidative stability (\%)} = \frac{W_2}{W_0} \times 100 \quad (6)$$

Where W_0 was initial weight before Fenton's test, W_2 was the residual weight after immersing COF membranes in Fenton's reagent for 1 h at 80 °C.

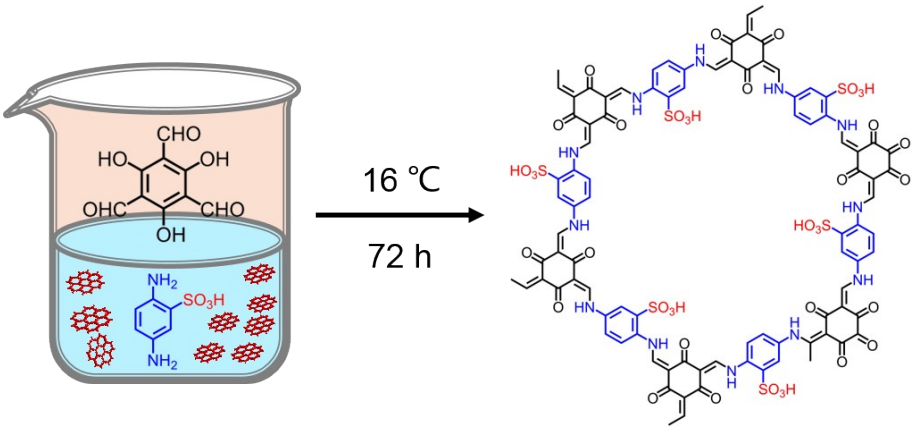

Fig. S1. Schematic illustration for the synthetic route of SCOF nanosheets.

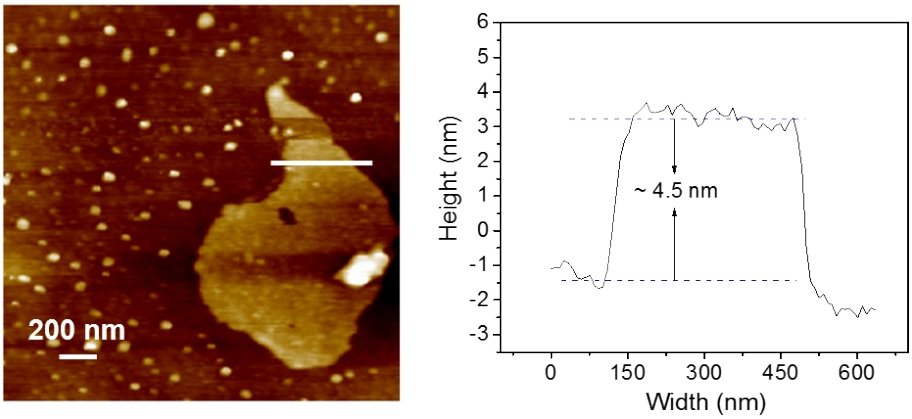

Fig. S2. AFM image of SCOF nanosheets.

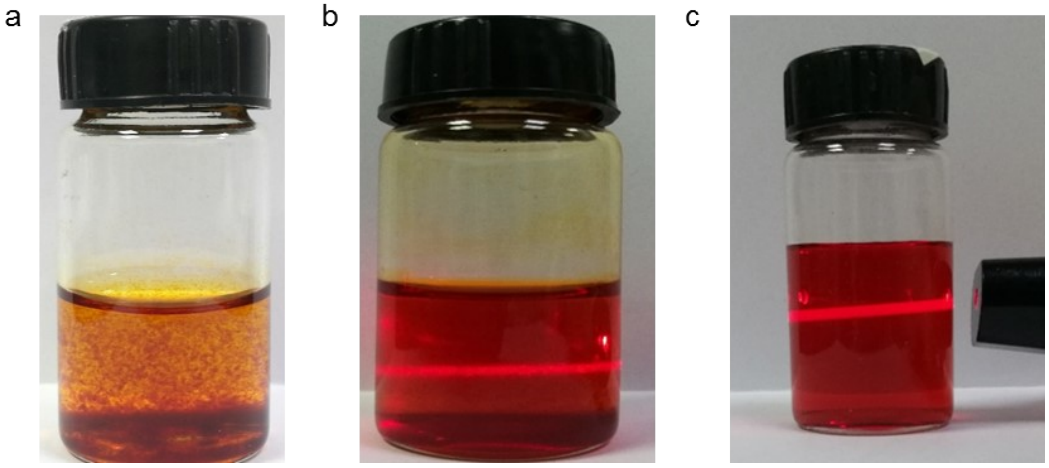

Fig. S3. Digital photos of (a) SCOF and PGQD solutions mixed together directly, (b) SCOF and PGQD solutions mixed together after that the pH values of SCOF nanosheets suspension and PGQD solution were tuned above 7.0, (c) original SCOF nanosheets suspension.

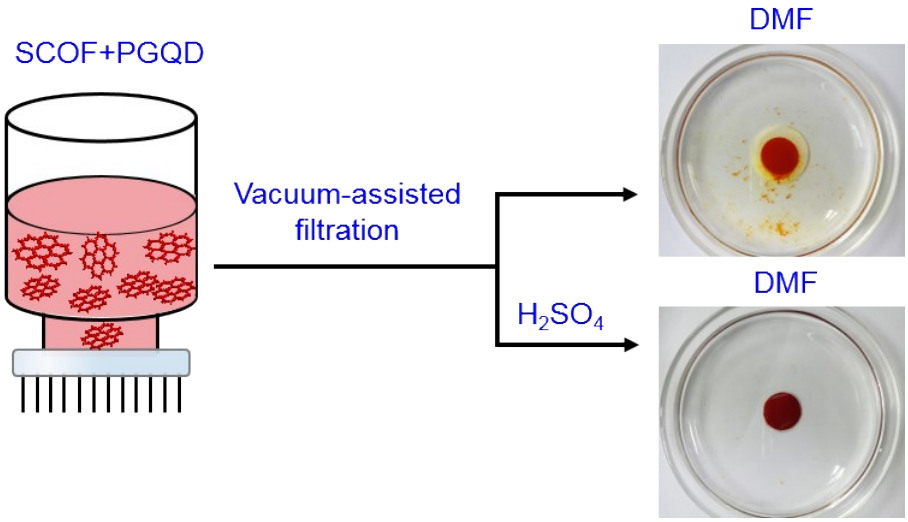

Fig. S4. Schematic diagram of the preparation process of SCOF/PGQD membranes.

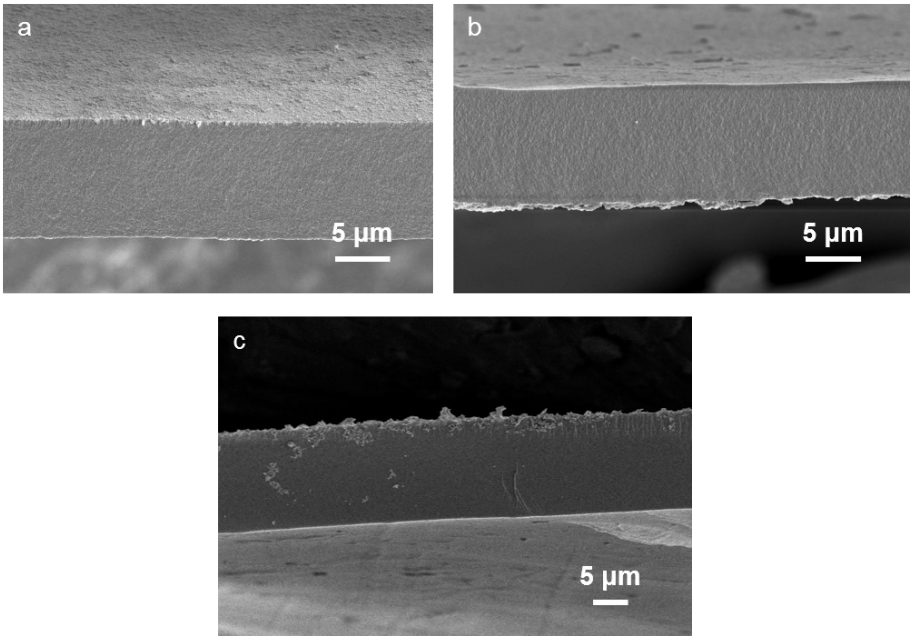

Fig. S5. Cross-section SEM images of (a) SCOF/PGQD-12.5, (b) SCOF/PGQD-25, (c) SCOF/PGQD-50 membranes.

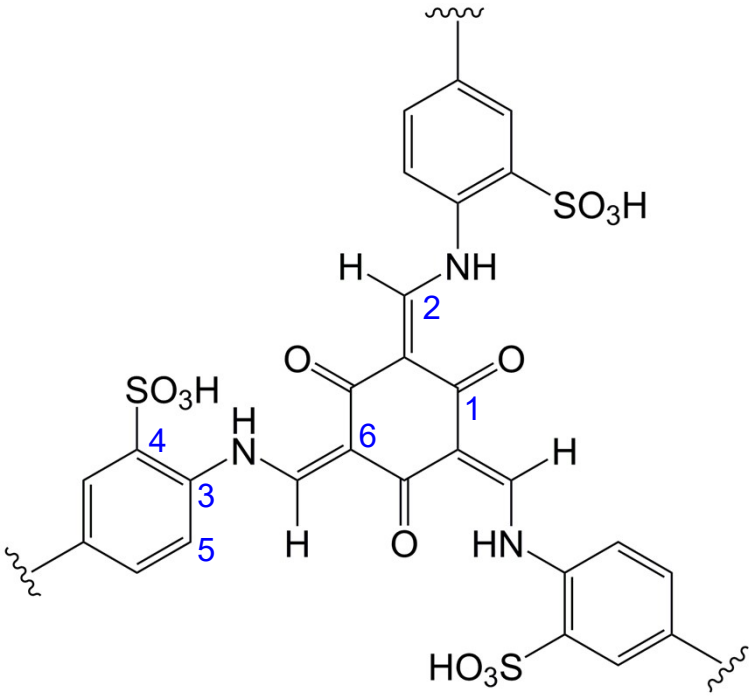

Carbon number	Chemical shift (ppm)
1	184
2	149
3	135
4	125
5	118
6	107

Fig. S6. Solid-state ^{13}C NMR spectrum and peak assignments of SCOF membrane.

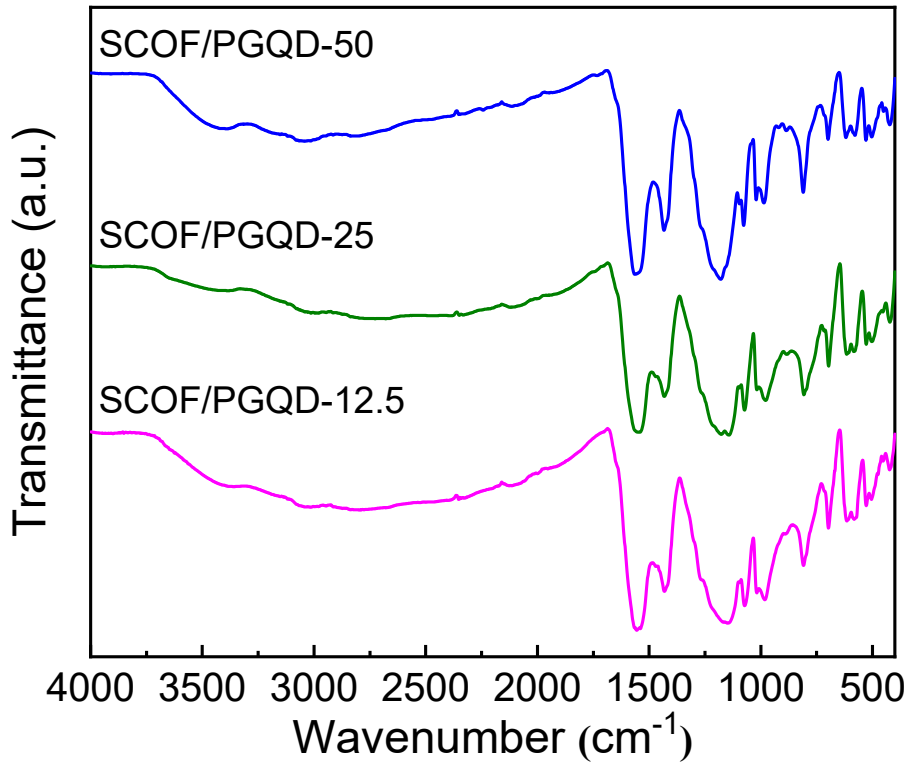

Fig. S7. FTIR spectra of SCOF/PGQD-X membranes.

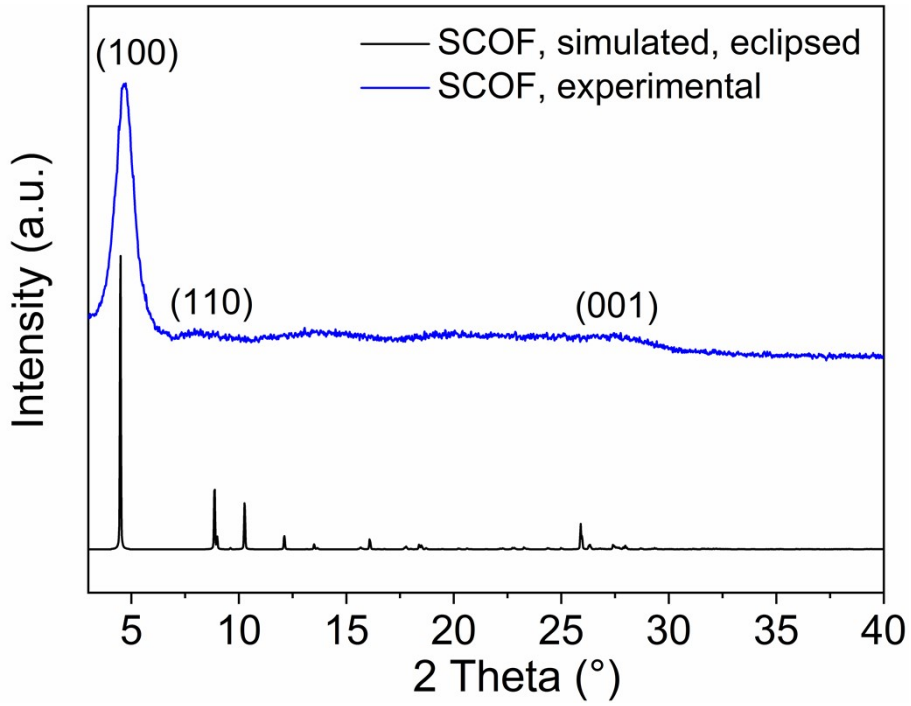

Fig. S8. The experimental XRD pattern of SCOF membrane (blue) compared with simulated eclipsed stacking model (black) in the reported work.

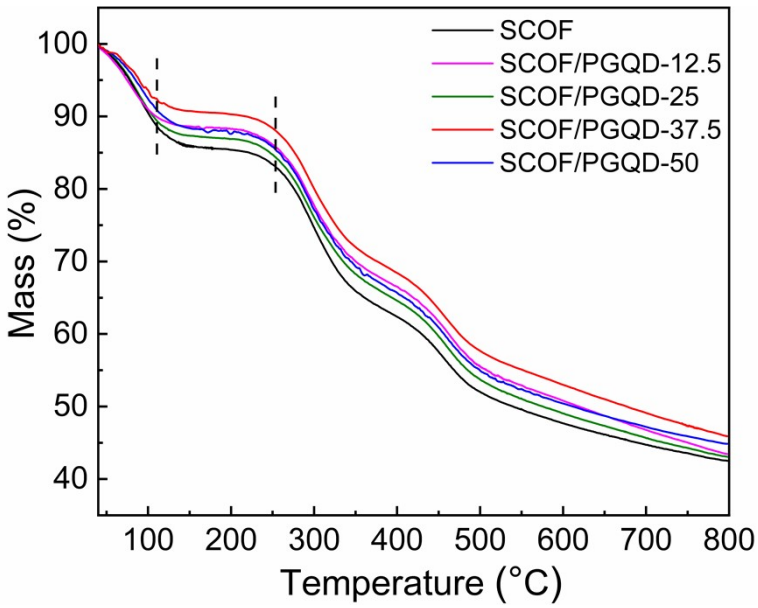

Fig. S9. TG curves of SCOF and SCOF/PGQD-X membranes.

Table S1. Oxidative stability of SCOF and SCOF/PGQD-X membranes

Membrane	Oxidative stability[a] (wt %)
SCOF	87.88 ± 0.8
SCOF/PGQD-12.5	90.48 ± 0.6
SCOF/PGQD-25	93.75 ± 0.5
SCOF/PGQD-37.5	94.12 ± 0.6
SCOF/PGQD-50	93.33 ± 0.9

[a.] Residual weight percentage of the membranes after immersing in Fenton's agent for 1 h.

Table S2. Properties of the COF membrane in comparison with PEMs reported in literature

Membranes	Proton conductivity (mS cm^{-1})	Mechanical stability (MPa)	IEC (mmol g^{-1})	Reference
Nafon	90 (80 °C, 100% RH)	17.8	-	[1]
CBA/Nafon–PVA4h	110 (80 °C, 100% RH)	20.3	-	[1]
RN-PQD-5%	243 (80 °C, 100% RH)	8.29	0.72	[2]
RN-GQD3-5%	145 (80 °C, 100% RH)	5.20	0.82	[2]
Nafion/FGO	220 (80 °C, 100% RH)	24	1.00	[3]
Nafion/Z-COF	220 (80 °C, 100% RH)	26.5	0.85	[4]
SP@PVA/PEI/C2-30	561 (80 °C, 100% RH)	40	0.37	[5]
SPEEK/HPW/GO	119.04 (80 °C, 100% RH)	26.86	1.45	[6]
SPEEK/S-UiO-66@GO-10	268 (70 °C, 95% RH)	53.5	1.70	[7]
SPAES/SPTA-GO	412.5 (80 °C, 90% RH)	53.8	2.46	[8]
SPAES-2CST3	128.1 (90 °C, 100% RH)	50.0	1.42	[9]
PBI/SPAEK-SPOSS-1%	63 (80 °C, 0% RH)	24.4	-	[10]
GO/SGQD-PA-400	324.0 (75 °C, 100% RH)	65.0	3.03	[11]
GO/SC[8]A-30%	327.0 (80 °C, 100% RH)	73	1.97	[12]
PGO-1	102 (80 °C, 98% RH)	29.1	2.5	[13]
GO/MMT/SPVA-60	326.0 (80 °C, 100% RH)	180.7	1.638	[14]
IPC-COF	380 (80 °C, 98% RH)	91.2	3.2	[15]
PTSA@TpAzo COFMs	78 (80 °C, 95% RH)	16	-	[16]
SCOF/PGQD-37.5	923 (90 °C, 100% RH)	129.4	3.96	This work

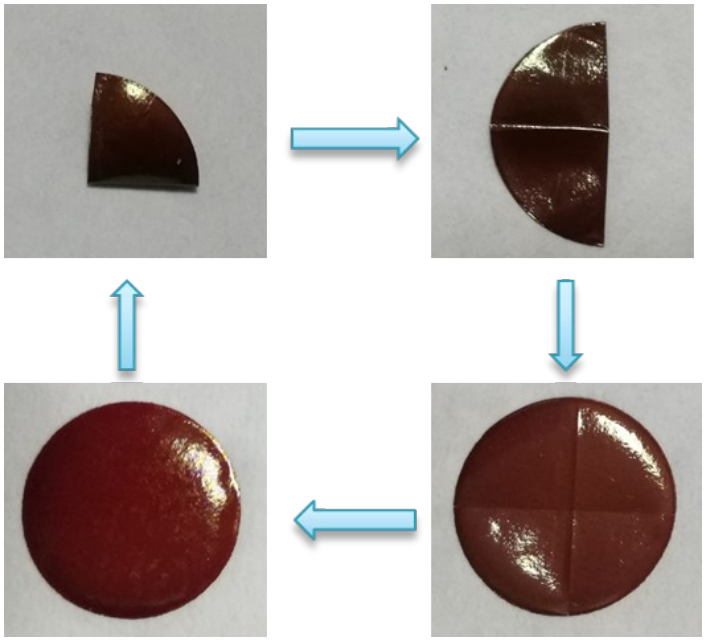

Fig. S10. Digital photos of SCOF/PGQD-37.5 membrane, showing the good flexibility of SCOF/PGQD-37.5 membrane.

Table S3. Swelling ratio and water uptake of SCOF and SCOF/PGQD-X membranes

Membrane	In-plane swelling ratio/ %		Through-plane swelling ratio /%		Water uptake/%	
	30 °C	60 °C	30 °C	60 °C	30 °C	60 °C
SCOF	1.1	1.1	9.9	10.7	27.7	40.4
SCOF/PGQD-12.5	1.0	1.1	9.6	10.6	31.0	50.4
SCOF/PGQD-25	1.3	1.3	10.2	11.0	35.7	57.1
SCOF/PGQD-37.5	1.5	1.5	11.7	12.3	46.2	65.3
SCOF/PGQD-50	1.6	1.7	13.0	14.7	47.1	71.5

Based on the operating temperature, proton exchange membrane fuel cells (PEMFCs) can be divided into two regimes: low–temperature PEMFCs working at 30–100 °C (LT–PEMFCs) and high–temperature PEMFCs working at 100–200 °C (HT–PEMFCs). HT–PEMFCs operating at high temperature and low humidity have gained great interest due to the following advantages (Table S4).[17-23]

(1) Electrode reaction kinetics

For LT-PEMFCs, the slowest electrochemical kinetics of Oxygen Reduction Reaction (ORR) determines the overall reaction rate. Thus, the cell voltage losses of the LT-PEMFC are mainly caused by the overpotential at the cathode. Compared to LT-PEMFCs, the ORR reaction kinetics of HT-PEMFCs can be greatly enhanced due to the higher working temperatures and the whole fuel cell performance can be improved significantly.

(2) Heat and water management

In the LT-PEMFCs, 40–50% of the energy is produced as heat and must be removed quickly to avoid over heat. Thus, a cooling system with a large dimension and weight is required to remove excess heat for maintaining the working temperature. While in the HT-PEMFCs, benefiting from the higher temperature difference between the fuel cell and ambient environment, the cooling system can be simplified and the waste heat can also be recovered. Therefore, the overall system efficiency can be increased significantly.

In the LT-PEMFCs, a dual-phase water system (i.e., liquid water/water vapor) exists when operating at lower temperature ($\leqslant$80 °C) under atmospheric pressure. This dual-phase water system needs to be carefully controlled for humidifying the membrane, which makes water management difficult. Increasing the operation temperature ($\geqslant$100 °C) can greatly simplify the water management because that there is only single water phase (i.e., water vapor) present. Both the simplified heat and water management will significantly reduce the overall cost.

(3) CO tolerance

In the LT-PEMFCs, the platinum (Pt) is used as catalyst for improving the electrochemical reaction. Notably, the Pt has a significant affinity for carbon monoxide (CO). If the concentration of CO in the H_2 fuel is excessive ($\sim$10 ppm), the fuel cell performance operating at low temperature will deteriorate largely due to the CO poisoning of Pt catalyst. As known, the adsorption of CO on Pt has high negative entropy, suggesting that low temperature will promote adsorption and high temperature will suppress the adsorption. Thus, operating the fuel cell at higher temperatures can greatly increase the CO tolerance as shown in Table S4.

Despite the great benefits of HT-PEMFCs, PEMs which can work efficiently at high temperatures (100–200 °C) and low relative humidity (RH = 25–50%) are still scarce. The development of PEMs with high proton conductivity and outstanding stability under the above harsh operation conditions remains a daunting challenge.

Table S4. The advantages of HT-PEMFCs compared to LT-PEMFCs

	Electrode reaction kinetics	Heat and water management	CO tolerance
LT-PEMFCs	In the LT-PEMFC, the ORR has the slowest electrochemical kinetics and the cell voltage losses are caused by the overpotential at the cathode.	working at temperatures ≤80 °C: (1) It requires a complex cooling system with a large dimension and weight; (2) A dual-phase water system makes water management difficult.	CO tolerance: 10–20 ppm at 80 °C, 1000 ppm at 130 °C, and 30,000 ppm at 200 °C[24, 25]
HT-PEMFCs	The reaction kinetics of ORR will be greatly enhanced at high temperature.	Operating above 100 °C: both the cooling system and water management can be simplified significantly.	

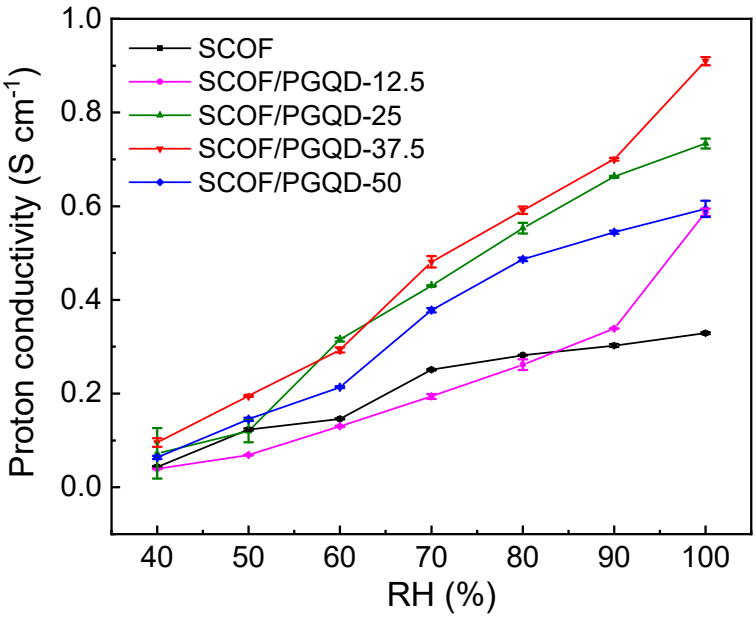

Fig. S11. Proton conductivity of SCOF and SCOF/PGQD-X membranes versus RH at 90 °C.

References

1. Y. Li, L. Liang, C. Liu, Y. Li, W. Xing and J. Sun, *Adv. Mater.*, 2018, **30**, e1707146.
2. W. Wu, Y. Li, J. Liu, J. Wang, Y. He, K. Davey and S. Z. Qiao, *Adv. Mater.*, 2018, **30**, e1707516.
3. X. He, G. He, A. Zhao, F. Wang, X. Mao, Y. Yin, L. Cao, B. Zhang, H. Wu and Z. Jiang, *ACS Appl. Mater. Interfaces*, 2017, **9**, 27676-27687.
4. Y. Li, H. Wu, Y. Yin, L. Cao, X. He, B. Shi, J. Li, M. Xu and Z. Jiang, *J. Membr. Sci.*, 2018, **568**, 1-9.
5. Y. Zhang, X. Zhang, P. Li, W. Wu, J. Lin, J. Wang, L. Qu and H. Zhang, *J. Mater. Chem. A*, 2020, **8**, 5128-5137.
6. F. Sun, L.-L. Qin, J. Zhou, Y.-K. Wang, J.-Q. Rong, Y.-J. Chen, S. Ayaz, Y. U. Hai-Yin and L. Liu, *J. Membr. Sci.*, 2020, **611**.
7. H. Sun, B. Tang and P. Wu, *ACS Appl. Mater. Interfaces*, 2017, **9**, 26077-26087.
8. J. Han, H. Lee, J. Kim, S. Kim, H. Kim, E. Kim, Y.-E. Sung, K. Kim and J.-C. Lee, *J. Membr. Sci.*, 2020, **612**.
9. L. Liu, Y. Pu, Y. Lu, N. Li, Z. Hu and S. Chen, *J. Membr. Sci.*, 2021, **621**.
10. J. Yang, X. Li, C. Shi, B. Liu, K. Cao, C. Shan, W. Hu and B. Liu, *J. Membr. Sci.*, 2021, **620**.
11. B. Shi, H. Wu, J. Shen, L. Cao, X. He, Y. Ma, Y. Li, J. Li, M. Xu, X. Mao, M. Qiu, H. Geng, P. Yang and Z. Jiang, *ACS Nano*, 2019, **13**, 10366-10375.
12. X. Mao, M. Xu, H. Wu, X. He, B. Shi, L. Cao, P. Yang, M. Qiu, H. Geng and Z. Jiang, *ACS Appl. Mater. Interfaces*, 2019, **11**, 42250-42260.
13. G. He, C. Chang, M. Xu, S. Hu, L. Li, J. Zhao, Z. Li, Z. Li, Y. Yin, M. Gang, H. Wu, X. Yang, M. D. Guiver and Z. Jiang, *Adv. Funct. Mater.*, 2015, **25**, 7502-7511.
14. G. He, M. Xu, J. Zhao, S. Jiang, S. Wang, Z. Li, X. He, T. Huang, M. Cao, H. Wu, M. D. Guiver and Z. Jiang, *Adv. Mater.*, 2017, **29**.
15. L. Cao, H. Wu, Y. Cao, C. Fan, R. Zhao, X. He, P. Yang, B. Shi, X. You and Z. Jiang, *Adv. Mater.*, 2020, **32**, e2005565.
16. H. S. Sasmal, H. B. Aiyappa, S. N. Bhange, S. Karak, A. Halder, S. Kurungot and R. Banerjee, *Angew. Chem. Int. Ed. Engl.*, 2018, **57**, 10894-10898.
17. A. Chandan, M. Hattenberger, A. El-kharouf, S. Du, A. Dhir, V. Self, B. G. Pollet, A. Ingram and W. Bujalski, *J. Power Sources*, 2013, **231**, 264-278.
18. Z. Guo, M. Perez-Page, J. Chen, Z. Ji and S. M. Holmes, *Journal of Energy Chemistry*, 2021, **63**, 393-429.
19. Y. Shao, G. Yin, Z. Wang and Y. Gao, *J. Power Sources*, 2007, **167**, 235-242.
20. J. Zhang, Z. Xie, J. Zhang, Y. Tang, C. Song, T. Navessin, Z. Shi, D. Song, H. Wang, D. P. Wilkinson, Z.-S. Liu and S. Holdcroft, *J. Power Sources*, 2006, **160**, 872-891.
21. J. A. Asensio, E. M. Sánchez and P. Gómez-Romero, *Chem. Soc. Rev.*, 2010, **39**, 3210-3239.
22. T. Xiao, R. Wang, Z. Chang, Z. Fang, Z. Zhu and C. Xu, *Progress in Natural Science: Materials International*, 2020, **30**, 743-750.
23. S. Bose, T. Kuila, T. X. H. Nguyen, N. H. Kim, K.-t. Lau and J. H. Lee, *Prog. Polym. Sci.*, 2011, **36**, 813-843.
24. Q. Li, R. He, J. O. Jensen and N. J. Bjerrum, *Chem. Mater.*, 2003, **15**, 4896-4915.
25. Q. Li, R. He, J.-A. Gao, J. O. Jensen and N. J. Bjerrum, *J. Electrochem. Soc.*, 2003, **150**, A1599.